

Star formation in outer rings of S0 galaxies. II.

NGC 4513 – a multi-spin ringed S0 galaxy.

I. Proshina¹, O. Sil’chenko¹, and A. Moiseev^{2, 1}

¹ Sternberg Astronomical Institute of the Lomonosov Moscow State University, University av. 13, 119234 Russia
 e-mail: ii.pro@mail.ru, olga@sai.msu.su

² Special Astrophysical Observatory of the Russian Academy of Sciences, Nizhnij Arkhyz, 369167 Russia
 e-mail: moisav@gmail.com

Received ..., 2019; accepted ..., 2019

ABSTRACT

Aims. Though S0 galaxies are usually thought to be ‘red and dead’, they demonstrate often star formation organized in ring structures. We try to clarify the nature of this phenomenon and its difference from star formation in spiral galaxies. The moderate-luminosity nearby S0 galaxy, NGC 4513, is studied here.

Methods. By applying long-slit spectroscopy along the major axis of NGC 4513, we have measured gas and star kinematics, Lick indices for the main body of the galaxy, and strong emission-line flux ratios in the ring. After inspecting the gas excitation in the ring using the line ratios diagnostic diagrams and have assured that it is ionized by young stars, we have determined the gas oxygen abundance by using popular strong-line calibration methods. We have estimated star formation rate (SFR) in the outer ring by using the archival Galaxy Evolution Explorer (GALEX) ultraviolet images of the galaxy.

Results. The ionized gas counterrotates the stars over the whole extension of NGC 4513 so being accreted from outside. The gas metallicity in the ring is slightly subsolar, $[O/H]=-0.2$ dex, matching the metallicity of the stellar component of the main galactic disc. However the stellar component of the ring is much more massive than can be explained by the current star formation level in the ring. We conclude that probably the ring of NGC 4513 is a result of tidal disruption of a massive gas-rich satellite, or it may be a consequence of a long star-formation event provoked by a gas accretion from a cosmological filament having started some 3 Gyr ago.

Key words. galaxies: structure – galaxies: evolution – galaxies, elliptical and lenticular – galaxies: star formation

arXiv:1912.12412v1 [astro-ph.GA] 28 Dec 2019

1. Introduction

Outer rings are common attributes of S0 galaxies by their definition (de Vaucouleurs 1959). The imaging statistics reveals that about 50% S0-S0/a galaxies possess outer stellar rings (Comeron et al. 2014; Laurikainen et al. 2011). Among those, about 50% are also seen in the UV-bands (Kostiuk & Sil’chenko 2015) so experiencing recent star formation and containing probably some amount of gas to fuel this star formation. The cool gas origin in S0s is still vague: though it is present in the most S0 galaxies (Welch & Sage 2003; Sage & Welch 2006; Welch, Sage, & Young 2010), but its spin is often decoupled from that of the stellar component (Bertola et al. 1992; Kuijken et al. 1996; Kannappan & Fabricant 2001; Pizzella et al. 2004; Davis et al. 2011; Serra et al. 2012), especially in rarefied environments (Katkov, Sil’chenko, and Afanasiev 2014; Katkov, Kniazev, and Sil’chenko 2015), that gives the evidence for recent gas accretion from outside (Thakar & Ryden 1996, 1998) along an arbitrary direction. Even much less is known about star formation in S0s providing *stellar* ring structures: it proceeds only in about the half of gas-rich lenticular galaxies (Pogge & Eskridge 1993), and the conditions provoking star formation occurrence in the gas accreted by S0s are not completely understood.

In this paper we will consider NGC 4513 – a northern-sky (R)SA0 galaxy of moderate luminosity, $M_H = -22.8$ (NED). The image of the galaxy taken from the Sloan Digital Sky Sur-

Table 1. Global parameters of the galaxy

Galaxy	NGC 4513
Type (NED ¹)	(R)SA0 ⁰
R_{25} , (NED+RC ²)	43'' or 7 kpc
B_T^0 (LEDA ³)	13.88
M_B (LEDA)	-18.99
M_H (NED)	-22.84
V_r (NED)	2304 km · s ⁻¹
Distance, Mpc (NED)	33
Inclination (LEDA)	59°
PA_{phot} (LEDA)	15.7°
$V_{rot} \sin i$, km · s ⁻¹ , (HI ⁴)	~ 170
σ_* , km · s ⁻¹ , (LEDA)	120
M_{HI}^4 , $10^9 M_\odot$	0.27

¹NASA/IPAC Extragalactic Database, <http://ned.ipac.caltech.edu>.

²Third Reference Catalogue of Bright Galaxies, de Vaucouleurs et al. (1991).

³Lyon-Meudon Extragalactic Database, <http://leda.univ-lyon1.fr>.

⁴Tang et al. (2008)

vey (SDSS) DR9 (Ahn et al. 2012) is shown in Fig. 1, left, and its main global parameters are given in Table 1. Earlier we have measured its stellar disc relative thickness (the ratio of the verti-

cal and radial scalelengths), by using our original method, and have obtained $q = 0.245 \pm 0.004$ (Chudakova & Sil'chenko 2014). Hence the outer stellar disc of NGC 4513 is somewhat thinner than the bulk of S0 stellar discs in rarefied environments (Chudakova & Sil'chenko 2014; Sil'chenko et al. 2020) among its morphological type (Hall et al. 2012). The galaxy is rather isolated: according to NED, there is no galaxies of comparable luminosity within 600 kpc from NGC 4513. An optical-band ring and the first spectral results for this galaxy were reported by Kostyuk (1975) and Kostyuk et al. (1981) long ago. The galaxy was observed in 21 cm line and was found to be a rather gas-rich S0, with $0.27 \times 10^9 M_{\odot}$ of the neutral hydrogen confined to the ring (Tang et al. 2008). In the Galaxy Evolution Explorer (GALEX) data, we have detected a UV-ring (Ilyina & Sil'chenko 2011) with the radius coupled to the optical ring size. Some preliminary description of the spectroscopic results was presented in Ilyina et al. (2014): it was there that we found that the gas in the outer ring counter-rotated the main stellar body. Now we will present a thorough analysis of our long-slit data and of the structure of the galaxy, including the inner part of NGC 4513 as well as star formation rate (SFR) estimates for the outer ring obtained from the imaging data in the UV retrieved in the public GALEX archive. The paper is the second one in the series about star formation in the S0 rings; earlier NGC 6534 and MCG 11-22-015, two galaxies with corotating detached outer rings, have been described by Sil'chenko et al. (2018b). As we have already found in our previous consideration of the gas kinematics in the S0 rings (Sil'chenko et al. 2019), the gas rotation in the plane coinciding with the stellar disc plane facilitates star formation. Indeed, in NGC 6534 and MCG 11-22-015 we have measured star formation rates of some $0.2 M_{\odot}$ per year that looks rather high for S0 galaxies. As we will show in the present paper, the counterrotating gas of NGC 4513 feeds much weaker star formation.

2. Observations and the data involved

Our long-slit spectral observations were made with a universal reducer SCORPIO-2 (Afanasiev & Moiseev 2011) at the prime focus of the Russian 6-m BTA telescope of the Special Astrophysical Observatory, Russian Academy of Sciences. NGC 4513 was observed on February 8, 2011, putting the 1''-slit along the isophote major axis, $PA(\text{slit}) = 15$ deg, with the total exposure time of 4800 sec (4×1200 sec). The seeing during these observations was poor, $FWHM \approx 3.5$ arcsec. We used the VPHG1200 grism having the maximum of effectivity at $\lambda \approx 5400$ Å providing an intermediate spectral resolution $FWHM \approx 5$ Å (corresponding to the instrumental σ of 130 km s^{-1}), to obtain a spectrum in a wavelength region from 4000 Å to 7200 Å. This spectral range includes a set of strong absorption and emission lines making it suitable to analyze both stellar and gaseous kinematics of the galaxy and its resolved stellar populations. The slit is 6' in length allowing to use the edge spectra to subtract the sky background. The CCD E2V CCD42-90, with a format of 2048×4600 px, using in the 1×2 binning mode provided a spatial scale of $0.357''/\text{px}$ and a spectral sampling of $0.86 \text{ Å}/\text{px}$.

The data were reduced by a standard way using the IDL software package developed in the SAO RAS. At the edges of the slit we derived the sky background to subtract it from the galaxy spectra, by using the polynomial (with the degree of 4) fit of the sky background distribution along the slit at every wavelength. Inhomogeneity of the optics transparency and variations of the spectral resolution along the slit were taken into account by us-

ing the dawn spectrum with the high signal-to-noise acquisition. The stellar kinematics was calculated by cross-correlating the binned galaxy spectra with the spectra of HD 102328 – a K2.5-giant star observed the same night as the galaxy. The emission lines, namely, the $H\alpha$, $[\text{NII}]\lambda 6583$, $[\text{SII}]\lambda 6717, 6731$, and $[\text{OIII}]\lambda 5007$, were used to derive ionized-gas kinematics, by measuring baricenter positions of the lines; in the bins where the continuum is strong we applied Gauss-analysis to take into account effects of underlying absorption lines: $H\alpha$ as well as TiI under the $[\text{OIII}]\lambda 5007$. For the latter purpose, we binned the spectra along the slit to reach signal-to-noise ratio higher than 50-70, and then made Gauss-analysis of the line complexes:

- $[\text{NII}]\lambda 6548, 6583 + H\alpha(\text{emission}) + H\alpha(\text{absorption})$,
- $H\beta(\text{emission}) + H\beta(\text{absorption})$,
- $[\text{OIII}]\lambda 5007(\text{emission}) + \text{TiI}\lambda 5007, 5015(\text{absorption})$.

With this analysis we are also able to derive the flux ratios of the strong emission lines: $[\text{NII}]\lambda 6583$ to $H\alpha$, $[\text{OIII}]\lambda 5007$ to $H\beta$, $[\text{SII}]\lambda 6717$ to $[\text{SII}]\lambda 6731$, which have been used to diagnose the gas excitation mechanisms with the BPT-diagrams (Baldwin et al. 1981) and to determine electron density and also gas oxygen abundances for the emission-line regions where the gas is ionized by radiation of young stars. The detector sensitivity variations along the wavelength were corrected by observing a spectrophotometric standard star GRW+70d5824 during the same night.

To study the large-scale structure of the galaxy, we have involved the g - and r -band images from the SDSS DR9 archive (Ahn et al. 2012). To estimate the star formation rate in the ring, we have retrieved the GALEX data: NGC 4513 was deeply imaged by this space telescope on January 21, 2005, in the frame of the Guest Investigator program no. 1-045009 intended to observe another ring galaxy, VII Zw 466, projected onto the sky plane not far from NGC 4513. The total exposures of the GALEX observations were 4286 sec in the FUV-band and 8198 sec in the NUV-band.

3. The structure of NGC 4513

By using the g - and r -band images of NGC 4513 provided by the SDSS/DR9 archive (Ahn et al. 2012), we have undertaken isophotal analysis, with the algorithm analogous to ELLIPSE/IRAF, and then by fixing the isophote parameters, the position angle (PA) of the major axis and the ellipticity $1 - b/a$ of the outermost part of main body of the galaxy, $R = 15'' - 40''$, we averaged the surface brightness over the elliptical rings. The scatter of the individual ellipticity and position angle measurements around the mean values in the radius range of $R = 15'' - 40''$ allows to estimate the typical errors of $1 - b/a$ and PA in the low surface-brightness regions as less than 0.02 and $\sim 1^\circ$, correspondingly. Our logique which we follow during the analysis of galactic exponential discs is presented in detail by Sil'chenko et al. (2018a). The results of the isophote analysis – the radial profiles of the PA(major axis) and isophote ellipticity, – as well as the surface brightness profiles – are presented in Fig. 2. The local ellipticity maximum and a turn of the isophote major axis reveal the presence of a bar ending at $R \approx 8''$. From $R \geq 14''$ to $\sim 40''$ the surface brightness profile has a perfect exponential shape, and the isophote parameters stay constant; we conclude that it is an area of a large-scale exponential disc domination, since according to Freeman (1970), exponential stellar discs are indicated by obeying a single-scale exponential law over the radius range of more than twice exponential scalelengths. The radial scalelength of the exponential profile of the

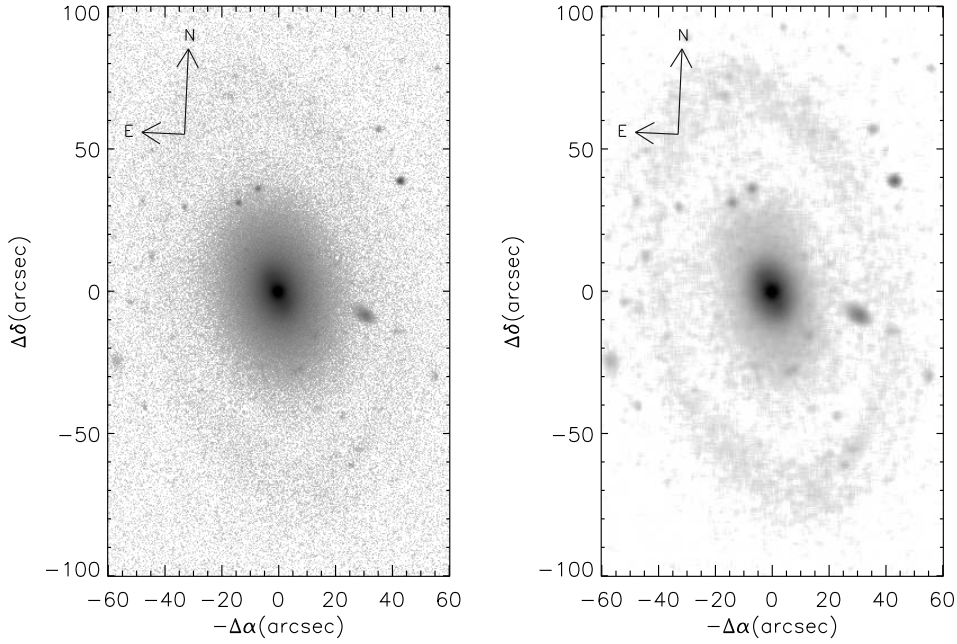


Fig. 1. The SDSS r -band image of NGC 4513 (*the left plot*) and the same image after the subtraction of the outer disc (*the right plot*) – see the Section 3 about the NGC 4513 image decomposition. The brightness scale is logarithmic and the same in both plots.

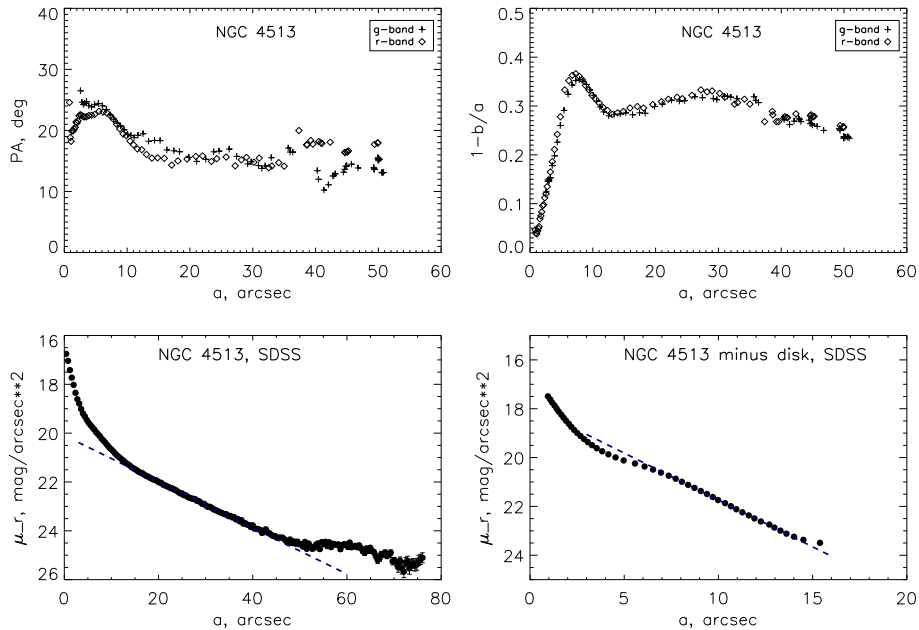


Fig. 2. The results of the photometric analysis of the SDSS/DR9 data: the results of the isophote analysis (*upper plots*) and the azimuthally averaged surface-brightness profiles of the full r -band image (*bottom left plot*) and of the image after the outer disc subtraction (*bottom right plot*). The blue dashed lines are the fitted exponential laws showing the areas of a disc and a pseudobulge domination in NGC 4513.

outer disc of NGC 4513 is $11''/5$, or 1.8 kpc. After subtracting the model outer exponential disc from the complete r -band image of NGC 4513, we see a residual image with a rather diffuse elongated surface brightness distribution (Fig. 1, right). By constructing its azimuthally averaged surface brightness profile with ellipse aperture parameters running along the radius, we obtain an exponential profile again, with the scalelength of 2.8 arcsec,

or ~ 0.5 kpc, in the radius range of $8''$ – $14''$ (Fig. 2, bottom right). We conclude that the bulge of NGC 4513 is in fact a pseudobulge which being a dynamically cold stellar system includes also a bar. In the radius range of $55''$ – $72''$ a surface brightness excess can be noted in Fig. 1 and also in the full surface brightness profile in Fig. 2, bottom left, – it is a signature of an outer stellar ring at the radius of about 10–12 kpc, beyond the outer edge of

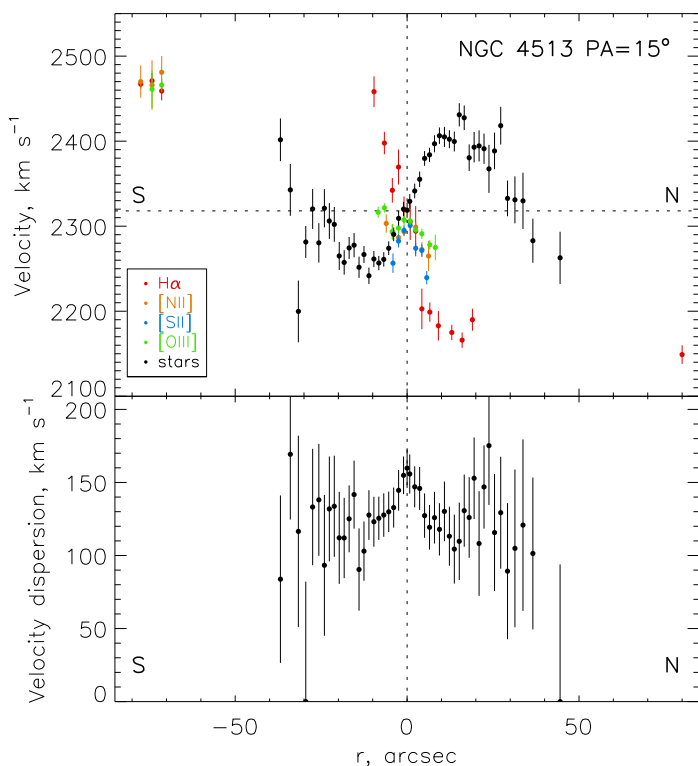


Fig. 3. The line-of-sight velocity profiles for the ionized gas and stars (*top*) and the stellar velocity dispersion profile (*bottom*) in NGC 4513 along its major axis. The black signs show the stellar component while various coloured signs refer to different emission lines of the ionized gas.

the main stellar disc, $R_{25} = 43''$, or 7 kpc (de Vaucouleurs et al. 1991).

4. Counterrotating gas and complex stellar component in NGC 4513

Figure 3 presents the line-of-sight velocity variations along the slit for the stars and ionized gas in NGC 4513. The velocities of the stellar component were determined by cross-correlating galaxy spectra with the spectrum of a K-giant star observed the same night with the same spectrograph configuration. The velocities of the ionized gas in the central part of the galaxy, $R < 10''$, were measured by Gauss-analysis of the line blends including the underlying absorption lines. In the more outer part of the main disc, the northern part, where the continuum is faint we calculated the baricenter wavelength position for $H\alpha$ at every radius. As Fig. 3 demonstrates, the ionized gas counterrotates the stars over the most extension of the galaxy. The stellar rotation curve starts to fall beyond $R \approx 15''$ and switches into a counterrotating regime at the outer edge of the disc, at $R \geq 30''$. It implies a possible existence of a secondary stellar component which may be related to the gas. Its presence may result in superposition of two counterrotating stellar components giving a null average rotation velocity at $R \approx 25''$, within the photometric disc-dominated area. To test this possibility, we have plotted a profile of the measured stellar velocity dispersion estimated as a σ of the stellar LOSVD (Fig. 3, *bottom*). Though our spectral resolution does not allow to measure reliably stellar velocity dispersions below 100 km s^{-1} expected in a disc, we can nevertheless feel qualitatively some increase of the visible

stellar velocity dispersion after the reverse of the rotation curve. Such behaviour of the stellar velocity dispersion profile supports our suggestion about two stellar-rotation components at our line of sight in the disc-dominated area. The rotation of the ionized gas in NGC 4513 is traced by measuring four strong emission lines (Fig. 3). In the central part of the galaxy, $R < 10''$, we see a rather flat segment of the gaseous velocity profile, consistent with a suggested gas slowdown at the bar edges. Further in the pseudobulge area the gas rotation curve rises steeply, and the gas velocities in the ring, consistent with the gas velocities at $R \geq 10''$, give evidence for a intrinsically flat character of the rotation curve over the full extension of the NGC 4513 disc. We do not see any emission lines between the inner edge of the disc and the outer ring; it is in line with the finding by Tang et al. (2008) on a prominent central depression in HI gas disc.

5. Stellar population properties

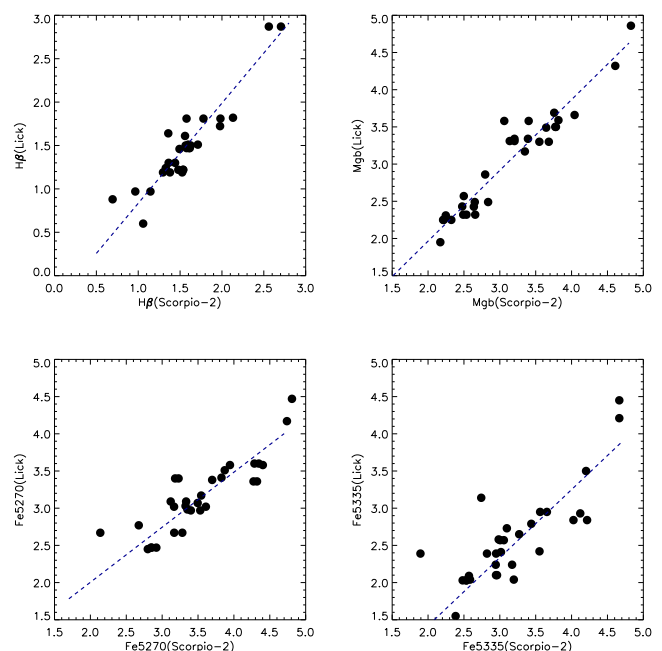


Fig. 4. The linear calibration of our instrumental Lick indices versus standard Lick indices for a sample of bright stars from Worthey et al. (1994).

To analyze the ages and chemical composition of the NGC 4513 stellar population, we have calculated the Lick indices $H\beta$, Mgb , $Fe5270$, and $Fe5335$, as well as the combined iron index, $\langle Fe \rangle \equiv (Fe5270 + Fe5335)/2$, and combined metallicity index, $[MgFe] \equiv \sqrt{Mgb/\langle Fe \rangle}$, along the radius by using our long-slit spectrum obtained with the SCORPIO-2 of the Russian 6m telescope. We prefer here the Lick index analysis because we expect non-solar ratio of the α -element-to-iron abundances, and popular now full-spectral fitting method is still restricted to the solar element pattern assumption. Firstly, we have calibrated our SCORPIO-2 index system to the standard Lick one by observing a sample of standard stars from the Worthey et al. (1994). The linear calibration dependencies are presented in Fig. 4. The scatter of individual stars around the linear dependencies, $\sim 0.2 \text{ \AA}$, is comparable to the accuracy of the Lick index measurements by Worthey et al. (1994).

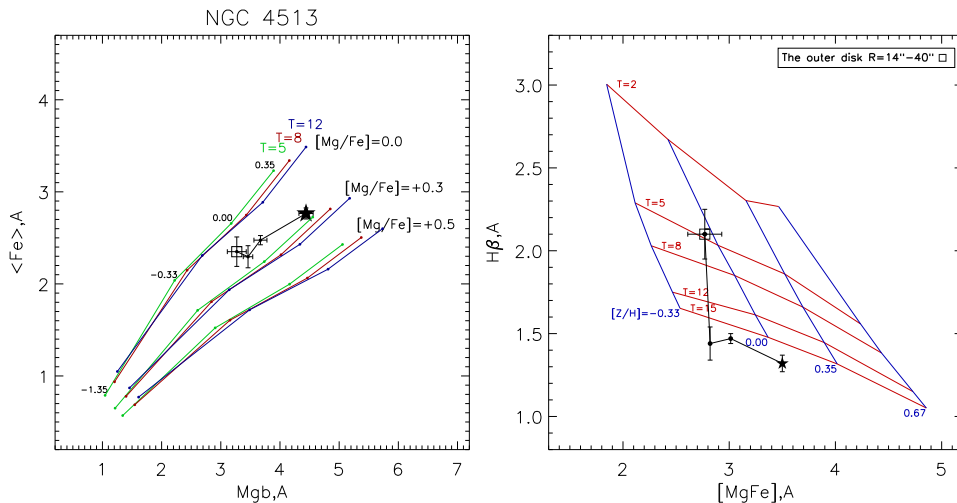


Fig. 5. Lick index-index diagrams for NGC 4513. The *left plot* represents Mg b vs iron index diagram which allows to estimate magnesium-to-iron ratio through the comparison of our measurements with the models by Thomas et al. (2003) for the different Mg/Fe ratios. By confronting the $H\beta$ Lick index versus a combined metallicity Lick index involving magnesium and iron lines (*right plot*), we solve the metallicity-age degeneracy and determine these stellar-population parameters with the SSP evolutionary synthesis models by Thomas et al. (2003). Five different age sequences (red lines) are plotted as reference frame; the blue lines crossing the model age sequences mark the metallicities of +0.67, +0.35, 0.00, -0.33 from right to left. A large black star corresponds to the central core, $R < 4''$, and then we go along the radius through the galaxy structure components: $R = 4'' - 8''$ (bar), $R = 8'' - 14''$ (pseudobulge), and $R = 14'' - 40''$ (disc). The point corresponding to the outer stellar disc is outlined by a large square.

Then we have estimated the SSP-equivalent ages and metallicities of the stellar populations along the radius of NGC 4513 by confronting our measurements of the Lick indices to the evolutionary synthesis models by Thomas et al. (2003). The $H\beta$ index was corrected for the emission contamination in the innermost part of the galaxy through measuring the $H\alpha$ emission-line equivalent width as it was described in Sil'chenko (2006). After that, broad radial bins corresponding to the photometric borders of the unresolved nucleus, $R < 4''$, the bar, $R = 4'' - 8''$, the pseudobulge, $R = 8'' - 14''$, and the large-scale stellar disc, $R = 14'' - 40''$, were defined. Our Lick indices were averaged within these radial bins. The results are presented in Fig. 5. The central part of the galaxy is homogeneously old and magnesium-overabundant. However, the large-scale stellar disc of NGC 4513 differs from the center of the galaxy as concerning the properties of the stellar population: it reveals a more prolonged history of star formation (its magnesium-to-iron ratio is closer to the solar value), which had stopped only a few billion years ago. The stellar metallicity of the galactic disc is only slightly subsolar. It is rather unusual for a lenticular galaxy in rarefied environments where the outer stellar discs are found to be coeval with the bulges (Katkov et al. 2015) or are older than the bulges (Sil'chenko et al. 2012). We may relate this unusual stellar age distribution again with the presence of the secondary, probably young stellar component which has come into the outer disc of NGC 4513 with the counterrotating gas accretion.

6. Gas-phase metallicity

Figure 6, *left*, shows the emission-line long-slit spectrum of NGC 4513 along its major axis, namely, its red portion with the continuum subtracted; and Fig. 6, *right*, – the BPT-diagram for the lowest (southern) location of the emission lines. One can clearly see gas-star counterrotation as well as the absence of the emission lines between the central part of NGC 4513 and its starforming ring which demonstrates emission lines at the $R = 70'' - 80''$.

In the central part of NGC 4513 the emission line $H\alpha$ is everywhere weak, and the strongest emission line is $[\text{NII}]\lambda 6583$. Such line ratio is consistent with the possible gas excitation by old stars (Binette et al. 1994; Byler et al. 2019) that is in agreement with the age of the stellar population in the central part of NGC 4513 (see Section 5). Otherwise the gas within $R < 8''$ could be excited by shock mechanism which is consistent with the bar presence. The bar contribution into the gas excitation is probably also manifested by strongly asymmetric electron density distribution along the slit: we have measured the trend of the sulfur line ratio, $[\text{SII}]\lambda 6717/\lambda 6731$, from 0.71 ± 0.07 to the south from the nucleus to 1.13 ± 0.04 to the north from the nucleus that corresponds to the n_e difference of about an order – 2400 cm^{-3} versus 300 cm^{-3} (Kewley et al. 2019).

In the ring the situation with a source of gas ionization could be different – here we expected the gas excitation by current star formation. We have plotted the emission-line ratios in the southern tip of the ring onto the BPT diagram (Fig. 6, *right*). Indeed, the strong-line ratios in the ring of NGC 4513 have appeared to lie below the theoretical border of the star formation calculated by Kewley et al. (2001) so the ionized gas of the ring may be mostly excited by young stars. But the prominent offset of the inner edge of the ring at the BPT-diagram with respect to the observational star formation sequence by Kauffmann et al. (2003) puts this region into the so called 'composite zone' revealing a noticeable contribution of diffuse interstellar gas (DIG) or shocks into the spectrum of the ionized gas of the ring. It means that not all strong-line methods of the gas oxygen determination are applicable to the inner edge of the ring in NGC 4513. Recent studies have shown that in the presence of DIG the most safe metallicity calibration is provided by the O3N2 method (Kumari et al. 2019), and we have decided to use just this method. By exploring both O3N2 calibrations from Pettini & Pagel (2004) and Marino et al. (2013), we have obtained for the inner edge of the ring of NGC 4513 $12 + \log(\text{O}/\text{H}) = 8.42 \pm 0.06$ dex. For the outer edge of the ring which is completely in the HII-region area of the BPT-diagram

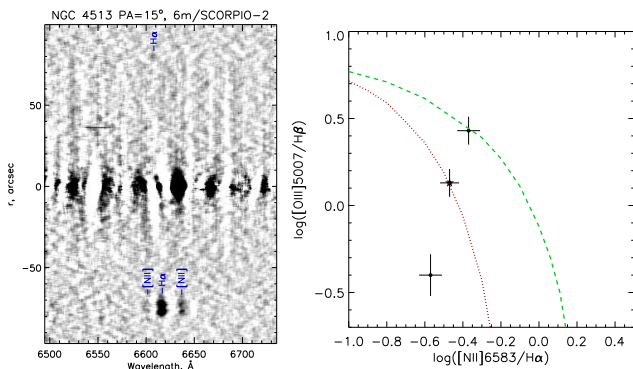


Fig. 6. Emission lines in the spectrum of NGC 4513: H α and the [NII] doublet (*left*) and the BPT-diagram for the southern tip of the ring (*right*.) At the BPT-diagram the known boundaries between HII-region excitation type and the others are plotted: the green dashed line is a theoretical boundary by Kewley et al. (2001), and the dotted red line is an empirical star-formation sequence from Kauffmann et al. (2003). We have plotted separately the inner edge of the ring, $R = 71.5''$ (*upper dot*), and the outer edge of the ring, $R = 76.5''$ (*lower dot*). The whole (integrated) ring is plotted by a black star.

and for the whole ring which falls exactly onto the star formation sequence by Kauffmann et al. (2003) we have used both N2 and O3N2 methods from the papers by Pettini & Pagel (2004) and Marino et al. (2013). We have obtained $12 + \log(\text{O}/\text{H}) = 8.57 \pm 0.06$ dex for the ring outer edge and $12 + \log(\text{O}/\text{H}) = 8.54 \pm 0.06$ dex for the whole ring. Together with the inner edge of the ring, these estimates imply the ring gas metallicity of about -0.2 dex with respect to the solar metallicity. It matches rather closely the stellar metallicity of the large-scale disc of NGC 4513 as reported in the Section 5. If to compare the gas oxygen abundance in NGC 4513 to the other outer rings of S0s studied by us (Proshina et al. 2019; Sil'chenko et al. 2019), it is just the same metallicity: for a sample of dozen gaseous outer rings in S0s, mostly with corotating kinematics (though in NGC 2551 the gas counterrotates), we have found $\langle [\text{O}/\text{H}] \rangle = -0.15$ dex (Sil'chenko et al. 2019).

7. Star formation in the outer ring of NGC 4513

NGC 4513 has been observed by the UV space telescope GALEX with rather large exposure times, so both the FUV- and NUV-images of the galaxy are deep, and the UV-appearance of the outer ring of NGC 4513 is rather prominent (Fig. 7). We have retrieved these FUV- and NUV-image from the MAST Archive and have overposed onto them an elliptical-ring aperture, slightly broader than the ring itself, to include all the ultraviolet flux, with the ellipticity matching the galaxy inclination, $1 - b/a = 0.3$. The aperture is centered onto the NGC 4513 nucleus, aligned with the outer isophote major axis, have the inner radius of $50''$ and the outer radius of $85''$ (Fig. 7). And then we have integrated the FUV- and NUV-fluxes within this ring aperture. The surrounding background was measured and subtracted. The fluxes in counts have been re-calculated into FUV- and NUV-magnitudes using the procedures described by Morrissey et al. (2007). Then we have corrected them for the foreground Galactic extinction by taking the NED A_B data for NGC 4513, and transformed into FUV- and NUV-luminosities by using the NED-provided distance of 33 Mpc to NGC 4513. We have applied the correction for the intrinsic dust by using the WISE/Band 4 ($22\mu\text{m}$) image of NGC 4513 cutted with the same elliptical-ring aperture. By obtaining the FUV- and NUV-

luminosities of the ring, we have transformed them into the star formation rates averaged over the last 100 and 200 Myr respectively, by using the calibrations proposed by Kennicutt & Evans (2012).

The resulting SFR estimate for the ring of NGC 4513 is 0.026 solar mass per year ($0.022M_{\odot} \text{ yr}^{-1}$ from the FUV-data and $0.030M_{\odot} \text{ yr}^{-1}$ from the NUV-data). We have compared this SFR with the total stellar mass of the NGC 4513 ring. Indeed, the SDSS data allow to estimate the integrated g -band and r -band magnitudes of the ring (in the same elliptical-ring aperture as the UV-signals). They have appeared to be $g(\text{ring}) = 15.16$ and $r(\text{ring}) = 14.61$. With the distance to NGC 4513 of 33 Mpc, we derive the absolute magnitude of the ring $M_g(\text{ring}) = -17.4$. By using the Bell et al. (2003) calibration of the mass-to-luminosity ratio against the colour, having $g - r(\text{ring}) = 0.55$, we assume $M/L_g = 2.14$. Then the total stellar mass of the ring is $2.26 \cdot 10^9 M_{\odot}$.

Now we can try different scenarios of the star formation history in the ring. To accumulate the stellar mass of $2.26 \cdot 10^9 M_{\odot}$ with the constant SFR in the ring of $0.026M_{\odot} \text{ yr}^{-1}$ – the rate which we have found from the UV-signal for the last 100-200 Myr, – the galaxy needs much more than the Hubble time. Under the opposite scenario, if the star formation history (SFH) declined exponentially and started some 3 Gyr ago, we would obtain the same stellar mass with a e-folding time of 0.6 Gyr which is rather typical for the S0 outer ring SFH (Proshina et al. 2019). In the former scenario we must conclude that not only the gas has been accreted from outside – a substantial amount of the stellar mass has been accreted too. In this case we deal not with pure gas accretion, but with tidal disruption of a gas-rich satellite. In the latter scenario, the galaxy can accrete only cold gas, but the mass of this gas, about $2.5 \times 10^9 M_{\odot}$, constitutes more than 10% of the total stellar mass of NGC 4513. The invisible source of the counterrotating gas in this case must be very abundant. In principle, it can be accretion of primeval gas from a cosmological filament because the current ratio of stellar-to-gas mass in the ring, ~ 8 , puts the chemical evolution of the ring of NGC 4513 into the 'gas-depleted' stage (Zahid et al. 2014; Ascasibar et al. 2015) so the current metallicity of the ionized gas must correspond to the saturation level which is close to the solar value (Zahid et al. 2014; Ascasibar et al. 2015), independently of the initial gas metallicity. It may explain the proximity of the gas oxygen abundance in the ring of NGC 4513 to a common value found by us for a number of other outer rings in S0 galaxies (Sil'chenko et al. 2019).

8. Discussion and conclusion: The origin of the ring in NGC 4513

Though according to our photometric analysis results (Fig. 2) NGC 4513 has a small bar, however we do not think that its outer ring relates somehow to the bar's resonances. Indeed, rings at outer Lindblad resonances show typical radii of 1.5–2 bar radius (Buta 2017), while in NGC 4513 the ratio $R(\text{ring})/R(\text{bar}) = 10 \pm 2$. Furthermore, the gas content of the ring counterrotates the main stellar body of the galaxy; this fact gives unambiguous evidence for an accretion nature of the ring.

The star formation in the ring is weak, $0.026M_{\odot} \text{ yr}^{-1}$ over a timescale of some 100 Myr. If such level of SFR remained roughly constant, the stellar content of the ring, some $2.3 \cdot 10^9 M_{\odot}$, could not be formed *in situ* and had to be also accreted together with the gas. If the SFH in the ring was strongly declined, with a e-folding time of ~ 0.6 Gyr during the last 3 Gyr, the stel-

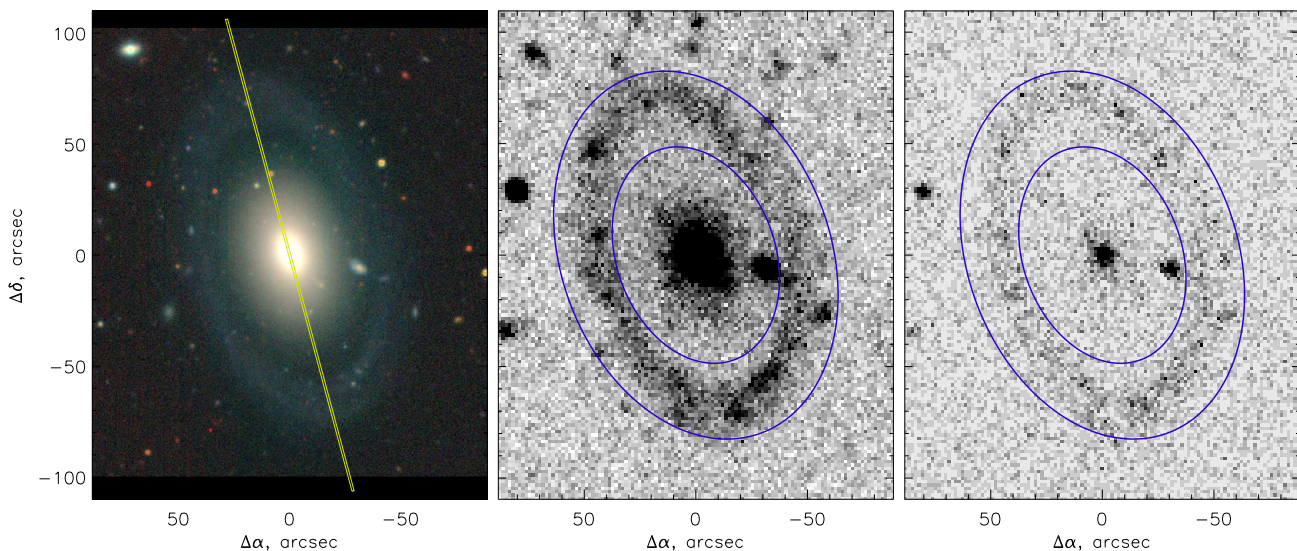


Fig. 7. The optical composite-color image (*left*), the product of the BASS survey, is taken from the Legacy Survey website (<http://legacysurvey.org>), the SCORPIO-2 slit position is overlapped; as well the GALEX maps of NGC 4513 are shown with the overposed apertures for the SFR estimates in the ring, NUV (*middle*) and FUV (*right*).

lar content of the ring could be formed *in situ*. The latter scenario implies that the stellar ring of NGC 4513 may be a consequence of a long star-formation event provoked perhaps by gas accretion from a cosmological filament as in the ring-like Hoag galaxy (Finkelman et al. 2011). In any case, the stars related to the counterrotating gas may contribute to the outer stellar disk of NGC 4513 which demonstrates the SSP-equivalent stellar ages of less than 5 Gyr together with the sharply falling rotation curve. The most probable scenario of the NGC 4513 ring acquisition is a tidal disruption of a gas-rich satellite. The ratio $\log M_{HI}/M_* \geq -0.9$ which we have found for the outer ring of NGC 4513 is indeed quite typical for satellite galaxies in gas-rich loose groups (Dzudzar et al. 2019). The environment of NGC 4513 corresponds to this scenario: according to the NED, the galaxy is rather isolated, it belongs to a loose group of 4 galaxy, and the nearest neighbour, emission-line dwarf PGC 2683704, is in 270 kpc and less massive by a factor of 30. Perhaps, a similar but a more close satellite was disrupted by NGC 4513 and had formed a ring with the radius corresponding to its orbital momentum.

Acknowledgements. We are grateful to the anonymous referee who has made a lot of very useful comments resulting in the paper improvement. The study of galactic rings was supported by the Russian Foundation for Basic Researches, grant no. 18-02-00094a. The work is based on the data obtained at the Russian 6m telescope of the Special Astrophysical Observatory carried out with the financial support of the Ministry of Science and Higher Education of the Russian Federation and on the public data of the SDSS (<http://www.sdss3.org>) and GALEX (<http://galex.stsci.edu/GR6/>) surveys. The NASA GALEX mission data were taken from the Mikulski Archive for Space Telescopes (MAST). The WISE data exploited by us were retrieved from the NASA/IPAC Infrared Science Archive, which is operated by the Jet Propulsion Laboratory, California Institute of Technology, under contract with the National Aeronautics and Space Administration. The NGC 4513 composite-colour optical image was taken from the Legacy Survey collection providing the imaging data of the BASS survey. BASS is a key project of the Telescope Access Program (TAP), which has been funded by the National Astronomical Observatories of China, the Chinese Academy of Sciences (the Strategic Priority Research Program "The Emergence of Cosmological Structures" Grant no. XDB09000000), and the Special Fund for Astronomy from the Ministry of Finance. The BASS is also supported by the External Cooperation Program of Chinese Academy of Sciences (Grant no. 114A11KYSB20160057), and Chinese National Natural Science Foundation (Grant no. 11433005). The Legacy Surveys imaging of the DESI footprint is supported by the Director, Office of Science, Office of High Energy Physics of the U.S. Department of Energy under Contract No. DE-AC02-05CH1123, by the

National Energy Research Scientific Computing Center, a DOE Office of Science User Facility under the same contract; and by the U.S. National Science Foundation, Division of Astronomical Sciences under Contract No. AST-0950945 to NOAO.

References

- Afanasiev, V. L., & Moiseev, A. V. 2011, *Baltic Astronomy*, 20, 363
Ahn, C. P., Alexandroff, R., Allende Prieto, C., Anderson, S. F., Anderton, T., et al., 2012, *ApJS*, 203, A12
Ascasibar, Y., Gavilán, M., Pinto, M., et al. 2015, *MNRAS*, 448, 2126
Baldwin, J. A., Phillips, M. M., Terlevich, R. 1981, *PASP*, 93, 5
Beasley, M. A., Brodie, J. P., Strader, J., et al. 2004, *AJ*, 128, 1623
Bell, E. F., McIntosh, D. H., Katz, N., Weinberg, M. D., 2003, *ApJS*, 149, 289
Bertola, F., Buson, L. M., Zeilinger, W. W., 1992, *ApJ*, 401, L79
Binette, L., Magris, C. G., Stasińska, G., Bruzual, A. G. 1994, *A&A*, 292, 13
Buta, R., Laurikainen, E., Salo, H., Knapen, J.H., 2010, *ApJ*, 721, 259
Buta, R. J., 2017, *MNRAS*, 470, 3819
Byler, N., Dalcanton, J. J., Conroy, C., et al. 2019, *AJ*, 158, A12
Chudakova, E. M., Sil'chenko, O. K., 2014, *Astronomy Reports*, 58, 281
Comerón, S., Salo, H., Laurikainen, E., et al. 2014, *A&A*, 562, A12
Davis, T. A., Alatalo, K., Sarzi, M., Bureau, M., Young, L. M., et al., 2011, *MNRAS*, 417, 882
de Vaucouleurs, G. 1959, *Handbuch der Physik*, 53, 275
de Vaucouleurs, G., de Vaucouleurs, A., Corwin, H. G. Jr., Buta, R. J., Paturel, G., Fouque, P., 1991, *Third Reference Catalogue of Bright Galaxies*, Springer-Verlag: Berlin/Heidelberg/New York, 2069 pp.
Dzudzar, R., Kilborn, V., Meurer, G., et al., 2019, *MNRAS*, 483, 5409
Finkelman, I., Moiseev, A., Broash, N., Katkov, I. 2011, *MNRAS*, 418, 1834
Freeman, K. C. 1970, *ApJ*, 160, 767
Hall, M., Courteau, S., Dutton, A. A., et al., 2012, *MNRAS*, 425, 2741
Ilyina, M.A., Sil'chenko, O.K., 2011, *Astronomy Letters*, 37, 589
Ilyina, M. A., Sil'chenko, O. K., Afanasiev, V. L., 2014, *MNRAS*, 439, 334
Kannappan, S. J., Fabricant, D.G. 2001, *AJ*, 121, 140
Katkov, I. Yu., Sil'chenko, O. K., Afanasiev, V. L., 2014, *MNRAS*, 438, 2798
Katkov, I. Yu., Kniazev, A. Yu., Sil'chenko, O.K. 2015, *AJ*, 150, A124
Kennicutt Jr., R. C., Evans II, N. J. 2012, *Ann.Rev. A&A*, 50, 531
Kauffmann G., Heckman, T. M., Tremonti, Ch., Brinchmann, J., Charlot, S., et al., 2003, *MNRAS*, 346, 1055
Kewley, L. J., Dopita, M. A., Sutherland, R. S., Heisler, C. A., Trevena, J., 2001, *ApJ*, 556, 121
Kewley, L. J., Nicholls, D. C., Sutherland, R. S., et al. 2019, *ApJ*, 880, A16
Kostyuk, I. P. 1975, *Soobsheniya Spets. Astrofiz. Obs.*, 13, 45 [in Russian].
Kostyuk, I. P., Karachentsev, I. D., Kopylov, A. I., 1981, *Soviet Astronomy Lett.*, 7, 148
Kostiuk, I. P., Sil'chenko, O. K. 2015, *Astrophys. Bull.*, 70, 280
Kuijken, K., Fisher, D., Merrifield, M.R. 1996, *MNRAS*, 283, 543
Kumari, N., Maiolino, R., Belfiore, F., Curti, M., 2019, *MNRAS*, 485, 367

- Laurikainen, E., Salo, H., Buta, R., Knapen, J.H., 2011, MNRAS, 418, 1452
Marino, R. A., Rosales-Ortega, F. F., Sánchez, S. F., et al., 2013, A&A, 559, A114
Morrissey, P., Conrow, T., Barlow, T. A., et al., 2007, ApJS, 173, 682
Pettini M., Pagel B.E.J., 2004, MNRAS, 348, L59
Pizzella, A., Corsini, E. M., Vega Beltrán, J. C., Bertola, F. 2004, A&A, 424, 447
Pogge, R. W., Eskridge, P. B., 1993, AJ, 106, 1405
Proshina, I. S., Kniazev, A. Yu., Sil'chenko, O. K. 2019, AJ, 158, Aid.5
Sage, L. J., Welch, G. A., 2006, ApJ, 644, 850
Serra, P., Oosterloo, T., Morganti, R., Alatalo, K., Blitz, L., et al., 2012, MNRAS, 422, 1835
Sil'chenko, O. K. 2006, ApJ, 641, 229
Sil'chenko, O. K., Proshina, I. S., Shulga, A. P., Kuposov, S. E. 2012, MNRAS, 427, 790
Sil'chenko, O. K., Kniazev, A. Yu., Chudakova, E. M. 2018, AJ, 156, 118
Sil'chenko, O., Kostiuk, I., Burenkov, A., Parul, H., 2018, A&A, 620, id.L7
Sil'chenko, O. K., Moiseev, A. V., Egorov, O. V. 2019, ApJS, 244, Aid.6
Sil'chenko, O. K., Kniazev, A. Yu., Chudakova, E. M. 2020, AJ, submitted
Tang, Y.-W., Kuo, Ch.-Y., Lim, J., Ho, P. T. P., 2008, ApJ, 679, 1094
Thakar, A. R., Ryden, B. S. 1996, ApJ, 461, 55
Thakar, A. R., Ryden, B. S. 1998, ApJ, 506, 93
Thomas, D., Maraston, C., Bender, R. 2003, MNRAS, 339, 897
Welch, G. A., Sage, L. J., 2003, ApJ, 584, 260
Welch, G. A., Sage, L. J., Young, L. M., 2010, ApJ, 725, 100
Worthey, G., Faber, S. M., González, J.J., Burstein, D., 1994, ApJS, 94, 687
Zahid, H. J., Dima, G. I., Kudritzki, R.-P., et al. 2014, ApJ, 791, Aid.130